

# Revision of conservative lower bound on intergalactic magnetic field from Fermi and Cherenkov telescope observations of extreme blazars

Jeffrey Blunier<sup>1</sup>, Andrii Neronov<sup>1,2</sup>, Dmitri Semikoz<sup>1</sup>

<sup>1</sup> Université Paris Cité, CNRS, Astroparticule et Cosmologie, 75006 Paris, France

<sup>2</sup> Laboratory of Astrophysics, École Polytechnique Fédérale de Lausanne, 1015 Lausanne, Switzerland

June 30, 2025

## ABSTRACT

**Context.** Joint observations of extreme blazars with Fermi Large Area Telescope (LAT) and Imaging Atmospheric Cherenkov telescopes (IACT) have been previously used to derive lower bounds on intergalactic magnetic field (IGMF).

**Aims.** We update these previous bounds using a set of extreme blazars that are detected in the Very-High-Energy (VHE, photon energies above 100 GeV) band by both Fermi/LAT and IACTs.

**Methods.** We measure IGMF-dependent suppression of secondary delayed  $\gamma$ -ray flux from electron-positron pairs deposited in the intergalactic medium by VHE  $\gamma$ -rays interacting with Extragalactic Background Light.

**Results.** From overall 22 extreme blazars detected by Fermi/LAT and IACTs in the VHE band, seven have their spectral characteristics inconsistent with the possibility of zero magnetic field along their lines of sight, even under the most restrictive assumption that the sources have only switched on at the start of VHE band observations. Adopting this assumption, we derive a "conservative" lower bound on the IGMF strength at the level of  $\sim 2 \times 10^{-17}$  G. The tightest bound is imposed by the signal of 1ES 0502+675, a source that has not been considered in the IGMF analysis before. Our bound is comparable to the bound derived by MAGIC collaboration, but is weaker than that previously derived from analysis of Fermi/LAT and HESS telescope data, even though our dataset includes that data. We clarify the origin of this discrepancy.

## 1. Introduction

Very-High-Energy (VHE)  $\gamma$ -rays from distant blazars (a type of Active Galactic Nuclei with jets aligned along the line of sight) interact with optical-infrared Extragalactic Background Light (EBL) photons on their way from the source to the Earth and deposit electron-positron pairs in the intergalactic medium, mostly in the voids of the Large Scale Structure. The electrons and positrons subsequently lose energy via inverse Compton scattering of photons of Cosmic Microwave Background and EBL and produce secondary  $\gamma$ -ray emission detectable by  $\gamma$ -ray telescopes (Aharonian et al. 1994). In the absence of magnetic fields in the voids, the secondary  $\gamma$ -ray flux would be emitted in the direction of the primary  $\gamma$ -ray beam and provide an additional contribution to the blazar  $\gamma$ -ray flux. Inter-Galactic Magnetic Field (IGMF) present in the voids deflects the trajectories of electrons and positrons so that the secondary emission is not any more directed along the primary  $\gamma$ -ray beam, suppressing the secondary flux in an IGMF-dependent way (Plaga 1995; Neronov & Semikoz 2007). This suppression has been observed (Neronov & Vovk 2010) and used to establish the existence of non-zero magnetic field in the voids (Neronov & Vovk 2010; Taylor et al. 2011; Acciari et al. 2023a; Ackermann et al. 2018; Aharonian et al. 2023).

Acciari et al. (2023a) have derived a conservative lower bound  $B > 1.8 \times 10^{-17}$  G on the void IGMF based on non-observation of delayed secondary signal in the  $\gamma$ -ray flux of the blazar 1ES 0229+200, using a combination of data

of MAGIC, HESS and VERITAS Imaging Atmospheric Cherenkov Telescopes (IACT) and Fermi Large Area Telescope (LAT). The conservative assumption of Acciari et al. (2023a) was that this source was never active in the VHE  $\gamma$ -ray band before the start of historical observations with IACTs two decades ago. Even though this is most probably not the case (the activity time scales  $T$  of blazars span tens-to-hundreds millions years, as indicated by their large scale jets), it cannot formally be ruled out that a specific source has just "switched on" at the moment of birth of the VHE astronomy.

Aharonian et al. (2023) have considered a combination of Fermi/LAT data with the data of HESS IACT for five blazars and derived lower bounds on IGMF, gradually relaxing the assumptions about the activity cycles of those sources: decade long  $T \sim 10$  yr (similar to Acciari et al. (2023a)),  $T \sim 10^4$  yr or  $T \sim 10^7$  yr. The bounds derived by Aharonian et al. (2023) are much stronger, in particular for the "conservative" time scale  $T \sim 10$  yr,  $B > 7 \times 10^{16}$  G. In the specific case of 1ES 0229+200, the lower bound derived by Aharonian et al. (2023) is  $B > 4 \times 10^{-16}$  G, a factor-of-twenty better than that of Acciari et al. (2023a). This is surprising, given that the analysis of Acciari et al. (2023a) includes also most of the HESS data considered by Aharonian et al. (2023).

The flux of the secondary  $\gamma$ -ray emission from the intergalactic medium is determined by the level of the primary VHE source flux in multi-TeV energy range. This flux is maximized for the sources with hard VHE  $\gamma$ -ray spectra and high VHE flux extending without high-energy

cut-off in the TeV range. This source class is known as "extreme" blazars (Fossati et al. 1998). The VHE emission from the extreme blazars is believed to be produced via synchrotron-self-Compton mechanism, via up-scattering of the synchrotron photons by energetic electrons. The frequency of the high-energy cut-off in the synchrotron spectrum correlates with the energy of the cut-off in the  $\gamma$ -ray spectrum. The "extreme" blazars are those with the highest energy synchrotron cut-off frequencies (in excess of  $10^{17}$  Hz) (Chang et al. 2019). The extreme blazars detected in the VHE band, the "extreme TeV blazars" (Biteau et al. 2020), are the best targets for the IGMF analysis.

Neronov & Semikoz (2025) have compiled a catalog of VHE emitting AGN based on a long exposure of Fermi/LAT. This catalog lists 275 such AGN in the sky region at Galactic latitudes  $|b| > 10^\circ$ . The catalog includes 63 extreme blazars. 22 of them have already been detected by IACTs.

In what follows we consider the IACT detected extreme blazars to re-evaluate the "conservative" lower bound on IGMF. In parallel, we are able to clarify the origin of discrepancy between the bound derived by Acciari et al. (2023a) and Aharonian et al. (2023). Our analysis is an improvement on both works, because it profits from a better knowledge of the "best targets" for the IGMF analysis, that were not considered in these two works.

## 2. VHE detected extreme blazar set

Table 1 presents the list of extreme blazars detected in the VHE band by both Fermi/LAT and IACTs (Neronov & Semikoz 2025). As mentioned in the introduction, there are further 41 VHE detected extreme blazars reported by Neronov & Semikoz (2025), for which there is currently no IACT data available. For these sources we cannot yet judge if they provide promising targets for the IGMF analysis and we do not consider them in this work. We also do not consider the brightest source, Mrk 501, for which dedicated studies have found that the secondary flux is largely sub-dominant (Takahashi et al. 2012; Korochkin et al. 2021).

We have combined broad-band GeV-TeV spectra of the 21 sources from Table 1 by complementing Fermi/LAT measurements with measurement by IACTs reported in the literature (cited in the "Time" column of the table). To extract Fermi/LAT spectra we use the aperture photometry approach in the same way as Neronov & Semikoz (2025) (see Appendix A for details). We fit all the combined Fermi/LAT + IACT spectra with cut-off powerlaw model  $N(E/1 \text{ TeV})^{-\Gamma} \exp(-E/E_{cut})$  modified by the effect of absorption on EBL, taken from Saldana-Lopez et al. (2021). We derive values of the slope  $\Gamma$ , cut-off energy  $E_{cut}$  and normalization of the spectrum  $N$  for each source. The values of  $\Gamma$ ,  $E_{cut}$  are given in columns 5 and 6 of Table 1. For most of the extreme blazars, the spectrum extends well into the TeV energy range and we are only able to obtain a lower bound on the cut-off energy, as can be seen from the " $E_{cut}$ " column of the table.

## 3. Secondary emission from the intergalactic medium

The cut-off powerlaw fit to the source spectra corresponds to the physical model with "infinite" IGMF, i.e. with IGMF

field strong enough to completely suppress the secondary flux from the direction of the source. Another extreme is the case with zero IGMF. For each source, we attempt to fit such zero IGMF alternative model to the spectrum. In this model, the total flux is a sum of the primary source flux attenuated by the effect of pair production on EBL plus the secondary flux from the inverse Compton scattering by the electron positron pairs. In the absence of IGMF, the secondary flux is emitted in the same direction as the primary source flux and is contributing to the point source spectrum. There is also (almost) no time delay of the secondary signal, so that even if all the sources from Table 1 have only appeared on the sky 20 years ago (with the start of observations by IACTs), their signals should be accompanied by the secondary emission component. In a more general situation, the secondary  $\gamma$ -rays arrive with a delay (Neronov & Semikoz 2009)

$$T_d = 2 \times 10^2 (1+z)^{-5} \left[ \frac{E_\gamma}{100 \text{ GeV}} \right]^{-5/2} \left[ \frac{B}{10^{-16} \text{ G}} \right]^2 \text{ yr} \quad (1)$$

in the case of magnetic field with correlation length  $\lambda_B \gg l_e$ , where  $l_e$  is the cooling distance of electrons and positrons with respect to the inverse Compton scattering. Considering  $T \sim 16$  yr for our (over)conservative assumption about source activity time scale (the time span of Fermi/LAT data considered in our analysis), one arrives at an order-of-magnitude estimate of suppression of the secondary flux by the time delay of the secondary signal introduced by the presence of IGMF. From Eq. (1) one finds that the field with the strength  $B \sim 10^{-16}$  G suppresses the secondary flux by a factor  $\kappa = (T_d/T) \gtrsim 10$  in the energy range below  $E_\gamma = 100$  GeV.

To move beyond this order-of-magnitude estimate, we use CRbeam code for modeling of the secondary emission (Berezinsky & Kalashev 2016; Kalashev et al. 2023). We consider IGMF with correlation length  $\lambda_B = 1 \text{ Mpc} > l_e$  in the energy range of interest (Neronov & Semikoz 2009). The magnetic field is chosen to have Kolmogorov power spectrum down to the wave number  $k_{min} = 2\pi/(5\lambda_B)$ . We assume that the source switches on as a  $\theta$ -function at the start of the 10-year long interval and calculate the average secondary signal spectrum over the 10-year time period from the start of the source activity. This secondary spectrum is added to the attenuated primary source spectrum and the combined primary + secondary model spectrum is fit to the data.

The time delay  $T_d$  is related to the angle of misalignment of the arrival direction of the secondary  $\gamma$ -ray  $\theta$  as  $T_d \sim \theta^2 D$ , where  $D$  is the distance to the  $\gamma$ -ray source (Neronov & Semikoz 2009). The time delay of the order of 20 yr corresponds to the misalignment angle  $\theta \sim 10''$ , which is not resolvable with  $\gamma$ -ray telescopes. Given this fact, our model fitting is limited to the point source spectrum.

We compare the quality of fits of the data with the two alternative models (zero IGMF and infinite IGMF), using the  $\chi^2$  minimization. Table 1 provides the  $\chi^2$  values of the fits of the data with the cut-off powerlaw model of the intrinsic spectrum (i.e. with very large IGMF that completely suppresses the secondary flux),  $\chi_\infty^2$  and with the zero IGMF model,  $\chi_0^2$ . The  $\chi^2$  values are quoted together with the number of degrees of freedom (the number of spectral data points minus 3, which is the number of parameters of the cut-off powerlaw model). We judge the source useful for the IGMF analysis if the  $B = 0$  model is found to

Name	RA	Dec	Time	$\Gamma$	$E_{cut}$	$z$	$\chi_{\infty}^2/dof$	$\chi_0^2/dof$
1 SHBL J001355.9-185406	3.48	-18.912	41.5h H(1)	$1.68_{-0.12}^{+0.08}$	$0.8_{-0.3}^{+0.5}$	0.095	2.86/10	3.3/10
2 1ES 0229+200	38.214	20.316	144.1h H(2) 54h V(3) 145.5h M(4)	$1.63_{-0.05}^{+0.03}$	> 3.6	0.14	13.9/16	50.1/16
3 RBS 0413	49.972	18.753	48h V(5)	$1.72_{-0.17}^{+0.15}$	> 0.8	0.19	8.4/11	6.3/11
4 1ES 0347-121	57.354	-11.994	59.2h H(2)	$1.62_{-0.06}^{+0.05}$	> 0.9	0.188	29.1/16	37.1/16
5 1ES 0502+675	76.996	67.622	13h V(6)	$1.50_{-0.06}^{+0.03}$	> 1.0	0.314	17.7/14	85.3/14
6 PKS 0548-322	87.625	-32.277	53.9h H(2)	$1.80_{-0.03}^{+0.03}$	> 3.7	0.069	26.3/16	24.7/16
7 RGB J0710+591	107.623	59.135	22.1h V(7)	$1.76_{-0.05}^{+0.05}$	> 3.2	0.125	26.3/11	26.8/11
8 PGC 2402248	113.362	51.88	50h M(8)	$1.78_{-0.02}^{+0.03}$	> 1.3	0.065	9.2/11	9.7/11
9 RBS 0723	131.812	11.569	45.3h M(9)	$1.57_{-0.15}^{+0.12}$	> 0.2	0.198	6.2/8	5.2/8
10 MRC 0910-208	138.227	-21.045	17h H(10)	$1.75_{-0.08}^{+0.05}$	$0.6_{-0.2}^{+0.5}$	0.198	5.6/9	5.0/9
11 1ES 1101-232	165.909	-23.496	71.9h H(2)	$1.58_{-0.04}^{+0.04}$	> 2.0	0.186	10.3/15	44.2/15
12 RX J1136.5+6737	174.118	67.613	30h M(11)	$1.86_{-0.06}^{+0.06}$	> 1.0	0.134	7.9/10	7.7/10
13 1ES 1312-423	198.768	-42.611	150h H(12)	$1.69_{-0.12}^{+0.09}$	$0.8_{-0.4}^{+0.6}$	0.105	23.6/12	25.6/12
14 RBS 1366	214.494	25.724	56h V(13)	$1.71_{-0.09}^{+0.05}$	> 0.4	0.236	12.7/12	14.7/12
15 H 1426+428	217.129	42.678	73.5h V(14)	$1.795_{-0.015}^{+0.015}$	> 3.2	0.129	22.1/17	26.9/17
16 1ES 1440+122	220.698	12.013	53h V(15)	$1.77_{-0.08}^{+0.09}$	> 0.3	0.163	5.8/11	6.6/11
17 1ES 1727+502	262.078	50.227	508d L(16)	$1.83_{-0.06}^{+0.08}$	$2.0_{-0.4}^{+1.3}$	0.055	17.2/12	20.0/12
18 1ES 1741+196	266.008	19.596	30h V(17)	$1.96_{-0.06}^{+0.06}$	> 0.4	0.08	7.0/10	6.9/10
19 1RXS J195815.6-301119	299.581	-30.181	7.3h H(10)	$1.90_{-0.05}^{+0.03}$	> 0.9	0.119	5.5/11	5.7/11
20 MG2 J204208+2426	310.536	24.458	52.5h M(9)	$1.95_{-0.05}^{+0.05}$	> 0.6	0.104	14.1/9	13.7/9
21 H 2356-309	359.772	-30.637	150.5h H(2)	$1.63_{-0.05}^{+0.03}$	$1.5_{-0.5}^{+1.3}$	0.165	20.4/16	26.1/16

Table 1: List of sources. The 3rd and 4th column give source coordinates. The fifth column is information on already available exposure of different IACTS ("H" for HESS, "M" for MAGIC and "V" for VERITAS). The only exception is 1ES 1727+502, for which we mention LHAASO detection (letter "L" is for LHAASO). Sixth and seventh columns provide spectral parameters (spectral slope  $\Gamma$  and cut-off energy  $E_{cut}$ , in TeV). The last column provides the source redshift.

**References.** (1) H. E. S. S. Collaboration et al. (2013); (2) Aharonian et al. (2023); (3) Madhavan & VERITAS Collaboration (2013); (4) Acciari et al. (2023b); (5) Aliu et al. (2012); (6) Orr (2013); (7) Acciari et al. (2010); (8) Collaboration (2019); (9) Acciari et al. (2020); (10) Bony (de) et al. (2022); (11) Hayashida et al. (2016); (12) HESS Collaboration et al. (2013); (13) Ribeiro (2023); (14) Farrell (2022); (15) Archambault et al. (2016); (16) Cao et al. (2024); (17) Abeysekara et al. (2016).

be inconsistent with the data. Considering the magnetic field strength as an additional parameter, we consider the model with zero magnetic field inconsistent with the data if  $\Delta\chi^2 = \chi_0^2 - \chi_{\infty}^2 > 2.71$ .

### 3.1. Sources that do not yield constraints on IGMF

For most of the sources in Table 1 we were able to find an acceptable fit to the Fermi/LAT + IACT data using the  $B = 0$  model. We show spectra of these sources in Fig. B.1 in the Appendix. The spectrum of the primary source is shown by the dashed line and the secondary flux spectrum is shown by the dotted line. The sum of the attenuated primary source and the secondary source fluxes is shown by the solid line. As an example, the spectrum of the first source, SHBL J001355.9-185406, has a high-energy cut-off. This is the reason why the secondary flux expectation is low. The level of the secondary flux is factor-of-two lower than the primary source flux at GeV energy and a small adjustment of the slope of the primary source spectrum (compared to the model without the secondary flux component) is sufficient to make the model with the secondary flux consistent with the data. In most of the other cases the cut-off in the spectrum is not constrained, but the quality of the VHE data is insufficient for a good estimate of the secondary flux level. It is clear that improvement of the

quality of the VHE spectral measurements (e.g. via longer exposure with existing IACTs, or with the next-generation IACTs) can tighten the constraint on the intrinsic source spectrum shape, in particular, on the lower bound on  $E_{cut}$ . If the lower bound on  $E_{cut}$  moves toward higher energy, the level of the secondary flux increases and it can start to be too high to be compatible with Fermi/LAT measurements. This would make these sources useful for the IGMF analysis. If the improvement of the IACT data would yield measurement of  $E_{cut}$ , precise predictions for the secondary flux level and spectra shape would become possible, further improving the precision of the IGMF analysis.

Several sources that have been previously used to derive constraints on IGMF by Aharonian et al. (2023) are not constraining IGMF in our analysis, in spite of the fact that we are using the same Fermi/LAT + HESS data combination as Aharonian et al. (2023). From Fig. B.1 one can see that, contrary to Aharonian et al. (2023), we find that the spectra of these sources can be fit consistently with a model with zero IGMF. We explain the origin of this discrepancy in Appendix A.

### 3.2. Sources that yield constraints on IGMF

There are seven sources for which the fit with zero IGMF is incompatible with the data: 1ES 0229+200, 1ES 0347-

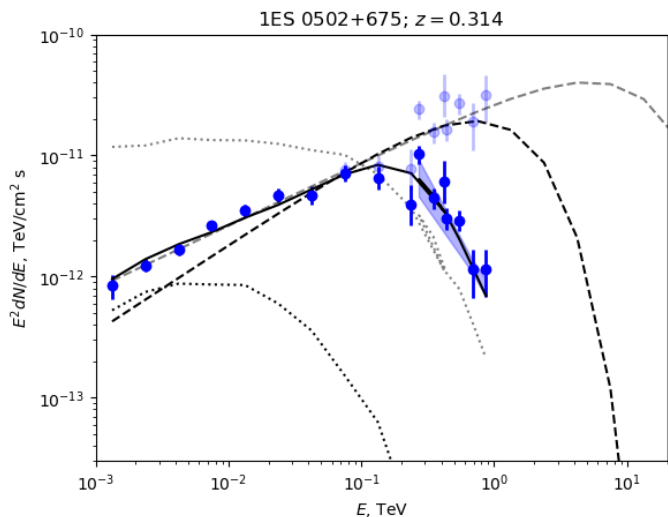


Fig. 1: Spectral modeling for 1ES 0502+675. Blue data points show Fermi/LAT and VERITAS data. Lighter color data points are corrected for the EBL absorption. Blue butterfly shows the measurement of the source spectrum from Abeysekara et al. (2019). Grey dashed line shows the best-fit intrinsic source cut-off powerlaw expected in the case of strong IGMF. Grey dotted line shows the secondary flux that is suppressed by the IGMF. Black curves show the model with minimal possible IGMF. Dashed line is the intrinsic source spectrum, dotted line is the secondary flux and solid line is the sum of the secondary and attenuated primary components.

Name	$B_{min}/10^{-17}$ G
1ES 0229+200	0.5
1ES 0347-121	0.07
1ES 0502+675	2.1
1ES 1101-232	0.6
H 1426+428	0.13
1ES 1727+502	0.02
H 2356-309	0.12

Table 2: Limits on IGMF from individual sources.

121, 1ES 0502+675, 1ES 1101-232, H 1426+428, 1ES 1727+502 and H 2356-309. Three of the sources: 1ES 0229+200, 1ES 0347-121 and 1ES 1101-232, have been used by Neronov & Vovk (2010) in the initial analysis that resulted in inference of existence of non-zero IGMF in the voids of the Large Scale Structure. H 2356-309 has been considered in the IGMF search by Aharonian et al. (2023). Three other sources, 1ES 0502+675, 1ES 1727+502 and H 1426+428 have not yet been considered in the IGMF analysis.

As an example, Fig. 1 shows the spectrum of 1ES 0502+675, with two alternative models. Gray dashed line shows the model without the secondary flux (with the secondary flux, represented by gray dotted line, suppressed by the IGMF). Black lines show the model with minimal possible magnetic field. In this case, the secondary flux (black dotted line) is only partially suppressed by the time delay due to IGMF and is contributing to the point source flux, shown by the black solid line. The minimal  $B$  models for the spectra of the other six sources are shown in Fig. 2.

Fig. 3 shows the  $\Delta\chi^2 = \chi^2(B|E_{cut}, \Gamma, N) - \chi^2_{\infty}$  of the model fits as a function of  $B$ , with the intrinsic spectrum parameters  $E_{cut}, \Gamma, N$  fixed to their best-fit values for each  $B$ . Following Avni (1976), we assume that  $\chi^2(B) = \chi^2(B|E_{cut}, \Gamma, N)$  is distributed as  $\chi^2_1$  with one degree of freedom and estimate one-sided 95% lower bound on  $B$  by requiring  $\Delta\chi^2 < 2.71$  for the models with acceptable  $B$ . In this sense, our approach is equivalent to that of Aharonian et al. (2023) where the same principle was applied to the profile likelihood as a function of  $B$ .

The strongest constraint on IGMF

$$B_{min,0502} > 2.1 \times 10^{-17} \text{ G} \quad (2)$$

stems from the spectral fit to the data of 1ES 0502+675 (Fig. 3). Neronov & Semikoz (2025) have noticed that this is the second-brightest VHE detected extreme blazar after Mrk 501. It has hard  $\gamma$ -ray spectrum extending up to TeV and as such it is a better candidate for constraining IGMF. Our analysis confirms this expectation. The IACT data considered in our analysis are from Orr (2013). From Fig. 1 one can see that the combined Fermi/LAT+VERITAS source spectrum does not show a signature of high-energy cut-off, once corrected for the EBL. The spectrum is hard, with the slope  $\Gamma$  consistent with the hardest possible slope of inverse Compton emission (1.5, see Table 1). The fit with minimal possible IGMF features even harder intrinsic powerlaw slope,  $\Gamma = 1.3$ . Table 2 lists the constraints on  $B$  imposed by the data on the other six sources. Fig. 3 shows the  $\Delta\chi^2$  profiles for all the seven sources.

Remarkably, the source 1ES 0229+200 that was found to yield strongest constraints in the HESS + Fermi/LAT analysis by Aharonian et al. (2023) is found to yield an order-of-magnitude weaker bound compared to Aharonian et al. (2023), in spite of the fact that the same HESS data are used in our analysis. We explain in Appendix A that this difference stems from the mismatches in the modeling of the secondary flux in the two analyses. Our secondary flux model rather matches that of Acciari et al. (2023b). The spectrum of the model with minimal possible IGMF in this case is shown in the left column of the top panel of Fig. 2.

Our bound on IGMF from 1ES 0229+200 data is broadly consistent with that derived by Acciari et al. (2023a) based on a combination of Fermi/LAT data with those of MAGIC, VERITAS and HESS. Acciari et al. (2023a) have noticed that 1ES 0229+200 is variable on the time scale of 20 yr of historical observations with IACTs. This variability can be taken into account self-consistently, by modeling the lightcurve of the delayed secondary flux using the knowledge of the primary source lightcurve. In our simplified version of analysis, we do not consider the details of the primary source variability. This explains the fact that our bound from 1ES 0229+200 data is somewhat weaker than that of Acciari et al. (2023a).

A bound similar to that from the 1ES 0229+200 data is provided by the 1ES 1101-232 data (see Fig. 3 and Table 2). Also this bound is significantly lower than the bound derived by Aharonian et al. (2023), with the discrepancy stemming from the modeling of the secondary signal. Four more sources: 1ES 0347-121, H 1426-428, 1ES 1727+502 and H 2356-309, provide lower bounds on IGMF that are much weaker than that imposed by the 1ES 0502+675 modeling. Weakness of the lower bound from 1ES 0347-121 can be partially understood as stemming from the bad quality

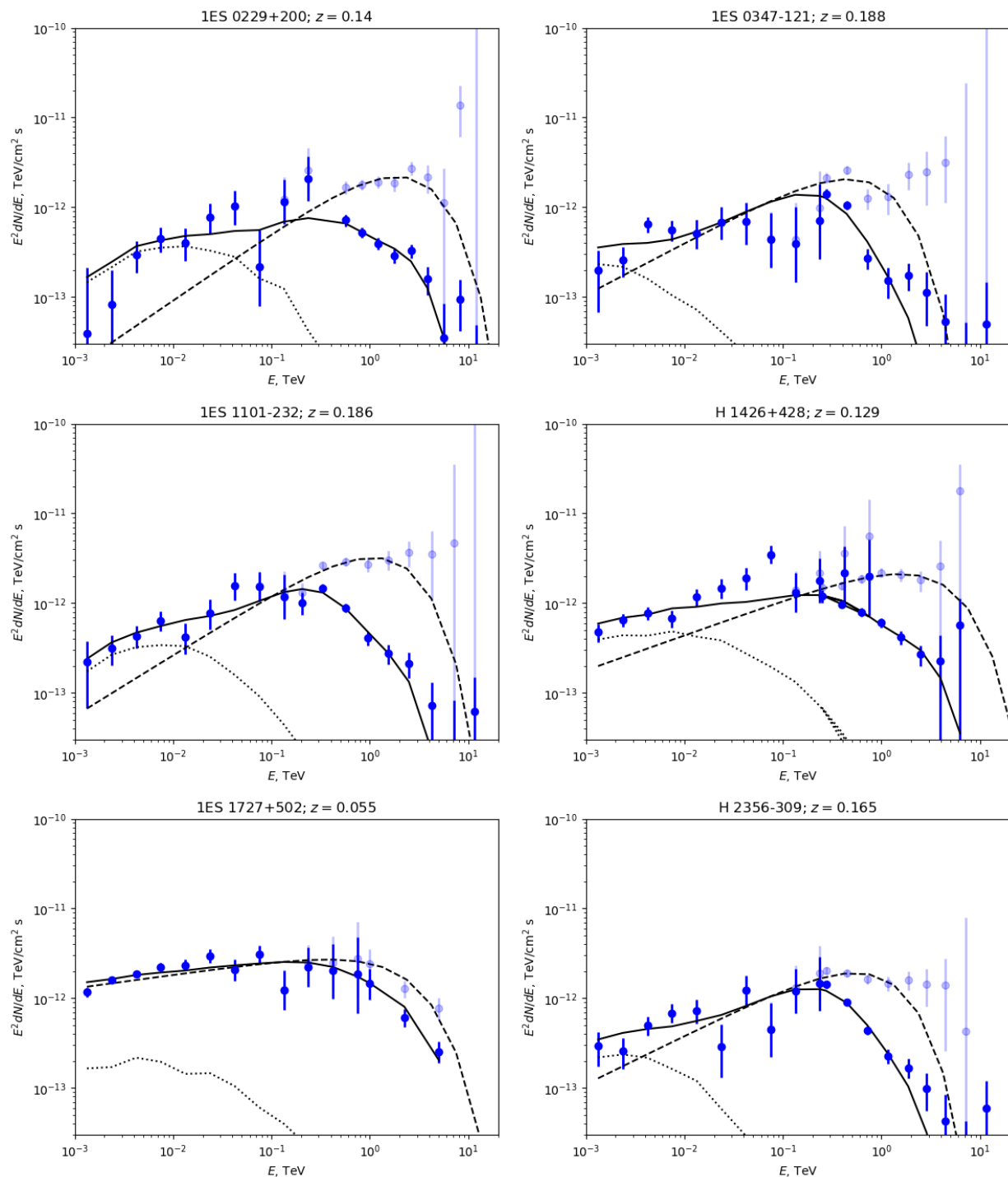


Fig. 2: Spectra of sources that provide constraints on IGMF. The data points are combinations of Fermi/LAT data with the IACT data for which references are listed in Table 1. The models correspond to the minimal possible field strength. The notations are the same as in Fig. 1.

of the spectral fits. Table 1 indicates that the  $\chi^2_\infty$  of the fit of the intrinsic source spectrum with a cut-off powerlaw model is 29.1 for 16 degrees-of-freedom (number of spectral measurement points minus the number of the model parameters). This means that the cut-off powerlaw model is actually inconsistent with the data at  $> 97\%$  confidence level. The spectrum of the source is shown in the top right panel of Fig. 2. One can see that the spectral data show large deviations from the powerlaw behavior and also HESS

data are not matching well the highest energy data points of Fermi/LAT. This can be because of variability of the source: Fermi/LAT measures the time-average source flux, while HESS performs snapshot observations on an irregular basis, that can catch some activity episodes and miss quiescent periods. In fact, the fit favors the model with magnetic field somewhat below  $10^{-17}$  G, as can be seen from the  $\Delta\chi^2$  plot for this source in Fig. 3. In this case the "hump" in the spectrum provided by the secondary flux component fits one

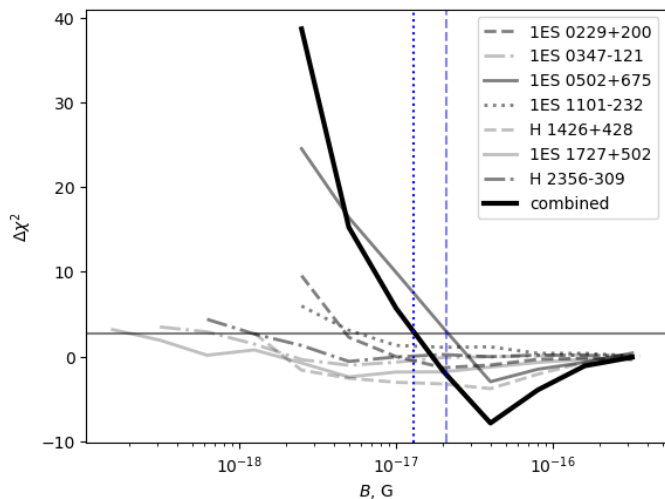


Fig. 3:  $\Delta\chi^2(B)$  profiles for the sources that constrain IGMF. Vertical blue dashed shows the lower bound on  $B$  from 1ES 0502+675, vertical blue dotted line shows the combined lower bound on IGMF from all sources. Horizontal line shows  $\Delta\chi^2 = 2.71$ .

of the deviations from the powerlaw in the data. The same is true for H 1426+428. The source spectrum is shown in the right column in the second row of Fig. 2. The fit favors certain value of  $B$  for which the secondary flux component fits a hump in the Fermi/LAT spectrum.

Following Aharonian et al. (2023), we also consider the combination of IGMF lower bounds by adding the  $\Delta\chi^2$  for all the seven sources. Similar to the single source analysis, for each value of  $B$ , we find the best fit intrinsic spectral parameters  $E_{cut,i}, \Gamma_i, N_i$  for each  $i$ th source separately, but the value of  $B$  is common for all sources. Adopting the approach of Avni (1976) also for this case, we assume that the cumulative  $\chi^2(B|E_{cut,1}, \Gamma_{cut,1}, N_1, \dots, E_{cut,7}, \Gamma_7, N_7)$  also follows the  $\chi^2$  statistics with one degree of freedom. Combination of data on all sources slightly relaxes the lower bound on IGMF, down to

$$B_{min,all} > 1.3 \times 10^{-17} \text{ G}. \quad (3)$$

This is explained by the fact that the bound from 1ES 0502+675 data is significantly stronger than the bounds from all other sources.

One can also notice in Fig. 3 that the cumulative  $\chi^2$  profile has a minimum at approximately  $B \simeq 4 \times 10^{-17}$  G, which is driven by the minimum in the  $\chi^2$  profile of 1ES 0502+576 and is further strengthened by the mild minima in the  $\chi^2$  profiles of other sources. We do not consider this minimum of the  $\chi^2$  profile as a measurement of IGMF, but rather as an artifact of our modeling approach. It is related to the (unrealistic) assumption that all seven sources considered in Fig. 3 have just switched on approximately ten years ago at the start of observations in the VHE  $\gamma$ -ray band. The IGMF with the strength  $B \simeq 4 \times 10^{-17}$  G induces the time delay that is of the order of 10 yr in the energy range  $E \sim 10$  GeV (see Eq. (1)). Delay time scale much longer than 10 yr in the GeV range produces significant suppression of the secondary flux at GeV, and a much more modest suppression in the 10 GeV range. This induces a curvature in the cascade spectrum around 10 GeV energy,

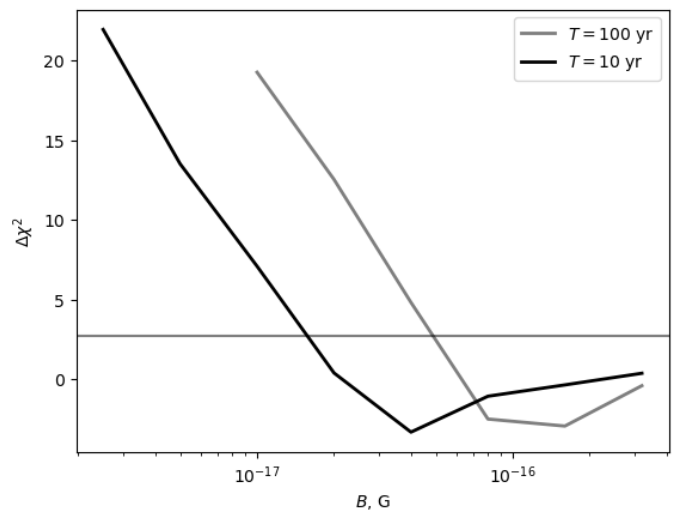


Fig. 4: Comparison of  $\Delta\chi^2(B)$  profiles for 1ES 0502+675 for two different assumptions about source activity period.

as can be seen from Fig. 1. The statistics of the Fermi/LAT signal in the 10 GeV range is sufficiently high, so that small deviations from the powerlaw behavior can be observed. The curved spectrum of the secondary emission component helps in modeling of the deviation of the spectrum from the powerlaw in this energy range. To demonstrate this effect explicitly, we show in Fig. 4 a comparison of the  $\Delta\chi^2$  profiles for 1ES 0502+675 for two different assumptions about the duration of the source activity cycle:  $T = 10$  yr and  $T = 100$  yr. One can see that the minimum of the  $\chi^2$  shifts toward higher magnetic field strength, because somewhat stronger field is required to achieve significant suppression of the secondary flux in the GeV range, while keeping only a moderate suppression at 10 GeV.

#### 4. Discussion and conclusions

We have used the set of extreme blazars detected in the VHE band by both Fermi/LAT and IACTs (Neronov & Semikoz 2025) to revise the lower bound on magnetic fields in the voids of the Large Scale Structure. This bound stems from the observation of the effect of suppression of the secondary  $\gamma$ -ray flux from electron-positron pairs deposited in the voids in result of interactions of VHE  $\gamma$ -rays with the optical and infrared photons of the EBL. Similar to Acciari et al. (2023a); Aharonian et al. (2023), we consider "conservative" (perhaps "over-conservative") assumption that sources have only "switched on" at the start of observations in the VHE band and the secondary emission is only suppressed because of the time delay of secondary flux caused by deflections of electrons and positrons in the IGMF.

In the specific case of the blazar 1ES 0229+200, considered by Acciari et al. (2023a), our bound is somewhat weaker than that derived by Acciari et al. (2023a), because we do not follow the details of source variability over the 20 years of source observations in the VHE band and assume that the source luminosity is represented by a  $\theta$ -function like switch-on followed by the constant luminosity on the 16-year time scale (representative of the time-averaged source luminosity). Comparing our limit on

IGMF with that derived by Aharonian et al. (2023), we find that we get a weaker lower bound, even though our modeling of source "switch-on" is the same as that of Aharonian et al. (2023). We argue that the origin of the mismatch of our and Acciari et al. (2023a) results with the results of Aharonian et al. (2023) stems from a discrepancy in the modelling of the secondary flux (see Appendix A for details).

Even though our limit on IGMF from the data on 1ES 0229+200 is weaker than that of Acciari et al. (2023a), we have identified another source, 1ES 0502+675, that provides a tighter lower bound on IGMF, at the level of  $B > 2.1 \times 10^{-17}$  G. We have checked that combination of the data on all sources that yield constraints on IGMF (seven in total) slightly worsens the lower bound on IGMF down to  $B > 1.3 \times 10^{-17}$  G. It is surprising that 1ES 0502+675 has not been considered before in the IGMF search and even no refereed journal publication<sup>1</sup> about the source spectrum has appeared since the detection of the source back in 2009 by VERITAS (Ong 2009). We were only able to find a conference proceedings report on the source spectrum. Given that the source provides the tightest constraints on IGMF in our analysis, we believe that a better characterization of its TeV band spectrum with longer IACT exposures would be useful. The source is very bright (the second-brightest VHE extreme blazar after Mrk 501, as noticed in Neronov & Semikoz (2025)), so that detailed characterization of its spectrum in the TeV band should be possible already with the current generation IACTs. There is clearly a potential for further tightening of the conservative lower bound on IGMF via extension of the IACT measurements in the energy range above 1 TeV.

In our analysis we have focused on IGMF with large correlation length  $\lambda_B > l_e$ . Nevertheless, we can extrapolate the results to the case of shows correlation length fields using prescriptions of Neronov & Semikoz (2009). The lower bound is independent of  $\lambda_B$  as long as  $\lambda_B > l_e$  and it scales as  $\lambda_B^{-1/2}$  in the  $\lambda_B < l_e$  range. The estimate of  $l_e$  in our analysis is identical to that of Acciari et al. (2023a),  $l_e \sim 0.1$  Mpc, so that our bound for the short correlation length field is

$$B \gtrsim 2.1 \times 10^{-17} \text{ G} \begin{cases} \left[ \frac{\lambda_B}{0.1 \text{ Mpc}} \right]^{-1/2}, & \lambda_B < 0.1 \text{ Mpc} \\ 1, & \lambda_B \geq 0.1 \text{ Mpc} \end{cases} \quad (4)$$

The short correlation length field bound is particularly interesting for the cosmological IGMF that may originate from cosmological phase transitions (Electroweak, quark confinement) (Durrer & Neronov 2013). For such fields the correlation length and strength are related by the "largest processed eddy" condition. There exist alternative estimates of the largest processed eddy scale, with the estimate of Banerjee & Jedamzik (2004) is  $\lambda \sim 1[B/10^{-8.5} \text{ G}] \text{ Mpc}$ . Hosking & Schekochihin (2023); Brandenburg et al. (2024) estimate it to be two-to-four orders of magnitude shorter. This gives a lower bound of  $\sim 10^{-14}$  G on the cosmological magnetic field under the assumption of Banerjee & Jedamzik (2004) largest processed eddy scaling and up to two orders of magnitude stronger

assuming Hosking & Schekochihin (2023) largest processed eddy scaling. The cosmological relic magnetic field with the strength close to this lower bound can, for example, be helical magnetic field that was responsible for the generation of baryon asymmetry of the Universe during the Electroweak cross-over (Kamada & Long 2016; Boyer & Neronov 2025), or it can be a non-helical field generated at quark confinement first order phase transition (Sigl et al. 1997).

The field at the level close to the lower bound derived above should be detectable using multiple techniques: through detection of delayed "pair echo" emission in the signals of AGN (Acciari et al. 2023a) and Gamma-ray Bursts (Miceli et al. 2024; Takahashi et al. 2011), or through the detection of extended emission around AGN (Neronov & Semikoz 2009; Ackermann et al. 2018; Aharonian et al. 2023). To identify best targets for such search, it is necessary to improve the knowledge of the intrinsic spectra of sources from Table 1: for most of them, no certain predictions for the secondary signal flux can be made because of uncertainty of the high-energy cut-offs in the spectra. This can be improved using the new generation of IACTs: CTAO (Cherenkov Telescope Array Consortium et al. 2019) and LACT (Zhang et al. 2025) that will have better sensitivity in the multi-TeV energy range. The information on the time-average intrinsic fluxes of the sources and on the presence of high-energy cut-offs in their spectra can also be provided by air shower arrays, like already operating LHAASO (Cao et al. 2024) and planned SWGO (Huentemeyer et al. 2019).

*Acknowledgements.* We would like to thank J.Biteau for clarifying discussions. This work has been supported in part by the French National Research Agency (ANR) grant ANR-24-CE31-4686.

## References

- Abeyssekara, A. U., Archambault, S., Archer, A., et al. 2016, MNRAS, 459, 2550  
Abeyssekara, A. U., Archer, A., Benbow, W., et al. 2019, ApJ, 885, 150  
Acciari, V. A., Agudo, I., Aniello, T., et al. 2023a, A&A, 670, A145  
Acciari, V. A., Agudo, I., Aniello, T., et al. 2023b, A&A, 670, A145  
Acciari, V. A., Aliu, E., Arlen, T., et al. 2010, ApJ, 715, L49  
Acciari, V. A., Ansoldi, S., Antonelli, L. A., et al. 2020, ApJS, 247, 16  
Ackermann, M., Ajello, M., Baldini, L., et al. 2018, ApJS, 237, 32  
Aharonian, F. et al. 2023, Astrophys. J. Lett., 950, L16  
Aharonian, F. A., Coppi, P. S., & Voelk, H. J. 1994, ApJ, 423, L5  
Aliu, E., Archambault, S., Arlen, T., et al. 2012, ApJ, 750, 94  
Alves Batista, R., Becker Tjus, J., Dörner, J., et al. 2022, J. Cosmology Astropart. Phys., 2022, 035  
Archambault, S., Archer, A., Barnacka, A., et al. 2016, MNRAS, 461, 202  
Avni, Y. 1976, ApJ, 210, 642  
Banerjee, R. & Jedamzik, K. 2004, Phys. Rev. D, 70, 123003  
Berezinsky, V. & Kalashev, O. 2016, Phys. Rev. D, 94, 023007  
Biteau, J., Prandini, E., Costamante, L., et al. 2020, Nature Astronomy, 4, 124  
Bony (de), M., Bylund, T., Meyer, M., et al. 2022, in 37th International Cosmic Ray Conference, 823  
Boyer, T. & Neronov, A. 2025, arXiv e-prints, arXiv:2504.07937  
Brandenburg, A., Neronov, A., & Vazza, F. 2024, A&A, 687, A186  
Cao, Z., Aharonian, F., An, Q., et al. 2024, ApJS, 271, 25  
Chang, Y. L., Arsioli, B., Giommi, P., Padovani, P., & Brandt, C. H. 2019, A&A, 632, A77  
Cherenkov Telescope Array Consortium, Acharya, B. S., Agudo, I., et al. 2019, Science with the Cherenkov Telescope Array Collaboration, M. 2019, MNRAS, 490, 2284  
Durrer, R. & Neronov, A. 2013, A&A Rev., 21, 62  
Farrell, K. 2022, PhD thesis, University of California at Davis

<sup>1</sup> A powerlaw spectral fit for this source is given in Abeyssekara et al. (2019). We show this fit in Fig. 1.

- Fossati, G., Maraschi, L., Celotti, A., Comastri, A., & Ghisellini, G. 1998, MNRAS, 299, 433
- H. E. S. S. Collaboration, Abramowski, A., Acero, F., et al. 2013, A&A, 554, A72
- Hayashida, M., Takami, H., Konno, Y., & Itoh, R. 2016, PoS, ICRC2015, 698
- H.E.S.S. Collaboration, Abramowski, A., Acero, F., et al. 2013, MNRAS, 434, 1889
- Hosking, D. N. & Schekochihin, A. A. 2023, Nature Communications, 14, 7523
- Huentemeyer, P., BenZvi, S., Dingus, B., et al. 2019, in Bulletin of the American Astronomical Society, Vol. 51, 109
- Kalashov, O., Korochkin, A., Neronov, A., & Semikoz, D. 2023, A&A, 675, A132
- Kamada, K. & Long, A. J. 2016, Phys. Rev. D, 94, 063501
- Korochkin, A., Kalashov, O., Neronov, A., & Semikoz, D. 2021, ApJ, 906, 116
- Madhavan, A. S. & VERITAS Collaboration. 2013, in International Cosmic Ray Conference, Vol. 33, International Cosmic Ray Conference, 1105
- Miceli, D., Da Vela, P., & Prandini, E. 2024, A&A, 688, A57
- Neronov, A. & Semikoz, D. 2025, arXiv e-prints, arXiv:2506.08497
- Neronov, A. & Semikoz, D. V. 2007, Soviet Journal of Experimental and Theoretical Physics Letters, 85, 473
- Neronov, A. & Semikoz, D. V. 2009, Phys. Rev. D, 80, 123012
- Neronov, A. & Vovk, I. 2010, Science, 328, 73
- Ong, R. A. 2009, The Astronomer's Telegram, 2301, 1
- Orr, M. 2013, arXiv e-prints, arXiv:1303.2142
- Plaga, R. 1995, Nature, 374, 430
- Ribeiro, D. 2023, arXiv e-prints, arXiv:2309.12230
- Saldana-Lopez, A., Domínguez, A., Pérez-González, P. G., et al. 2021, MNRAS, 507, 5144
- Sigl, G., Olinto, A. V., & Jedamzik, K. 1997, Phys. Rev. D, 55, 4582
- Takahashi, K., Inoue, S., Ichiki, K., & Nakamura, T. 2011, MNRAS, 410, 2741
- Takahashi, K., Mori, M., Ichiki, K., & Inoue, S. 2012, Astrophys. J. Lett., 744, L7
- Taylor, A. M., Vovk, I., & Neronov, A. 2011, A&A, 529, A144
- Zhang, Z., Yang, R., Zhang, S., et al. 2025, Chinese Physics C, 49, 035001

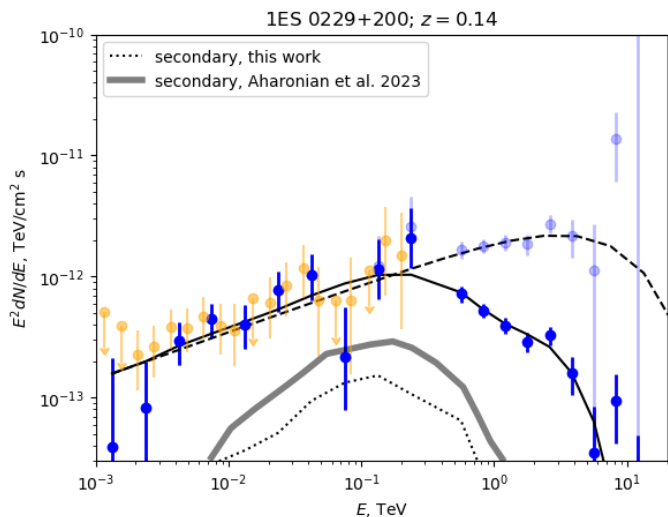


Fig. A.1: Comparison of the secondary flux from Aharonian et al. (2023) with our secondary flux model for the same parameters (magnetic field  $B = 3.2 \times 10^{-16}$  G, activity time  $T = 10$  yr, source 1ES 0229+200). Orange data points show the result of Fermi/LAT likelihood analysis by Aharonian et al. (2023).

## Appendix A: Modeling of the secondary flux and comparison with Aharonian et al. (2023)

We compute the secondary flux using the CRbeam code (Berezinsky & Kalashev 2016; Kalashev et al. 2023). We simulate a beam of photons in the energy range between 10 GeV and 30 TeV, with  $dN/dE \propto E^{-1}$  spectrum. For each secondary photon produced following the  $e^+e^-$  pair production followed by the inverse Compton scattering, we keep a memory of the primary photon. This allows us to calculate the secondary flux for any primary photon spectrum using single simulation of the  $E^{-1}$  spectrum, by simply weighting the secondary photons according to the energy of the primary photon. We propagate primary and secondary particles until they cross a sphere of the radius  $D$  equal to the distance to the source of interest. For each photon crossing the sphere, we calculate the angle between the direction of the photon and normal to the sphere, which corresponds to the angle of misalignment of the arrival direction of the secondary photons. We also notice the total path from the source for each photon crossing the sphere. This path, divided by the speed of light, gives the arrival time of all photons.

Fig. A.1 shows a comparison of our calculation of the secondary flux for  $T = 10$  yr activity time of 1ES 0229+200, for the magnetic field  $B = 3.2 \times 10^{-16}$  G with that of Aharonian et al. (2023). Our estimate of the secondary flux is by up to a factor-of-two lower than that of Aharonian et al. (2023). This difference does not stem from the discrepancies between CRbeam code that we use and CRpropa code (Alves Batista et al. 2022) used by Aharonian et al. (2023), because the two codes have been found to agree within the redshift range of interest (Kalashev et al. 2023). CRpropa code was also used in the modeling of the secondary flux by Acciari et al. (2023b), which which our calculations agree.

Our analysis is based on Fermi/LAT spectra extracted using the aperture photometry technique, as compared to the likelihood analysis used by Aharonian et al. (2023). To estimate the source flux in each energy bin, we use the knowledge of the 68% and 95% containment radii of the Fermi/LAT point spread function. If the total source signal in the energy bin is  $S$  and the background per square degree is  $b$ , the numbers of photon counts in the 68% and 95% containment circles are

$$\begin{aligned} S_{68} &= 0.68S + \pi(0.68^\circ)^2 b \\ S_{95} &= 0.95S + \pi(0.95^\circ)^2 b \end{aligned} \quad (\text{A.1})$$

so that the signal can be found from the measurements of  $S_{68}$  and  $S_{95}$ :

$$S = \frac{0.95^2 S_{68} - 0.68^2 S_{95}}{0.95^2 - 0.68^2} \quad (\text{A.2})$$

We use this estimate in the energy range below 50 GeV, where the background level is high. In the energy range above 50 GeV, the sources are mostly detected in the background-free regime and we assume that  $S = S_{95}/0.95$ . The aperture photometry approach has an advantage compared to the likelihood analysis approach in the "uncrowded" sky regions where there are no sources with overlapping signals. Contrary to the likelihood estimate, it does not depend on the sky model that has many parameters (of the Galactic diffuse emission, isotropic diffuse emission, distribution of point sources in the region of interest, choice of the spectral models and spectral parameters of those sources). We have checked that our aperture photometry spectra are consistent with those of the likelihood analysis by Aharonian et al. (2023). Fig. A.1 shows a comparison of the aperture photometry and likelihood analysis for 1ES 0229+200.

## Appendix B: Spectra of sources that do not yield constraints on IGMF

In this appendix we show spectral fits of the model with secondary flux for sources that do not currently yield constraints on IGMF. This can be either because the quality of the data is not sufficient for detection of the secondary flux or because the source spectrum has high-energy cut-off that suppresses the secondary flux. Fig. B.1 shows the spectra of such sources.

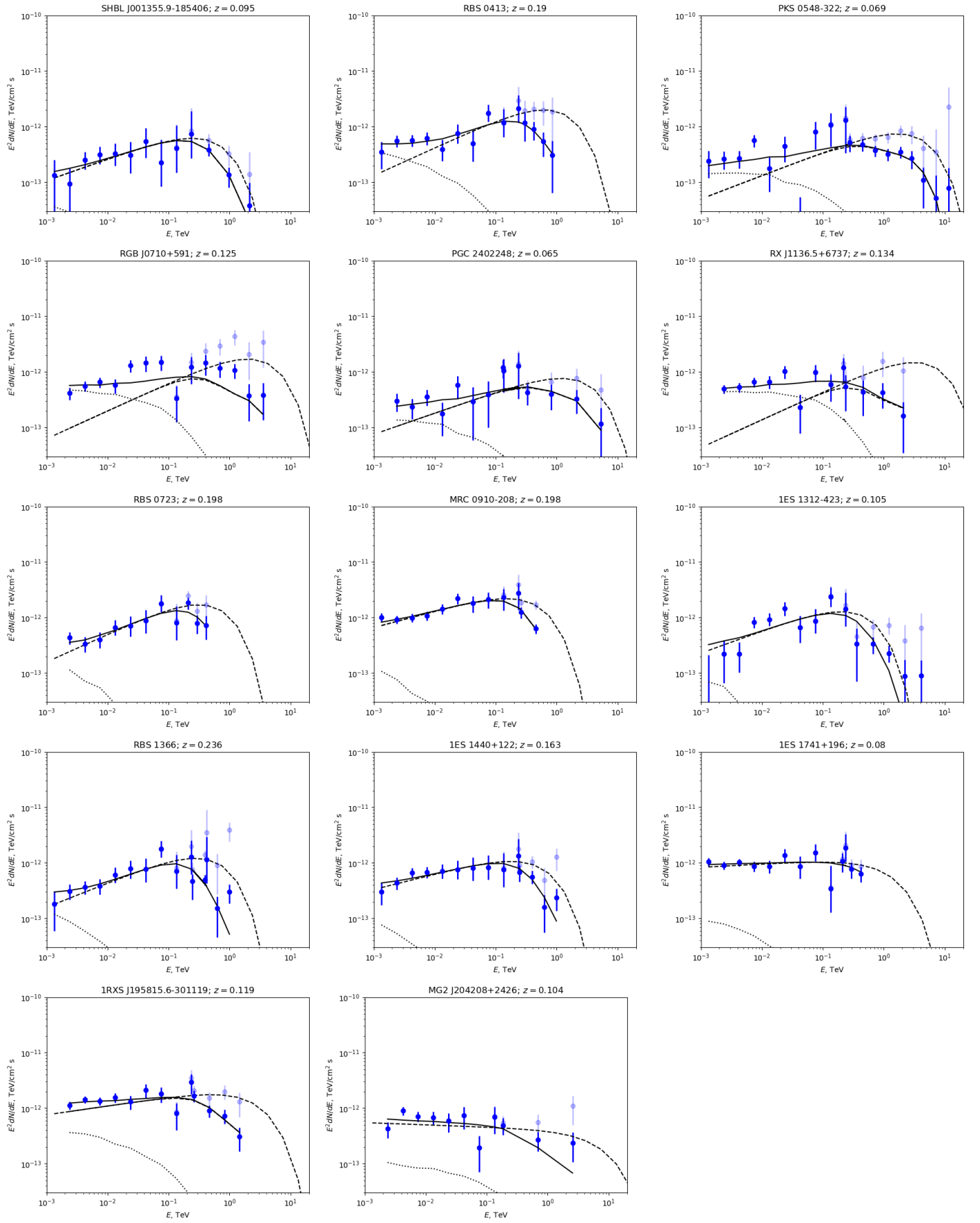


Fig. B.1: Same as in Fig. 2 but for other sources that do not yield constraints on IGMF.